HHS Public Access

Author manuscript

Nat Struct Mol Biol. Author manuscript; available in PMC 2016 October 25.

Published in final edited form as:

Nat Struct Mol Biol. 2016 June ; 23(6): 513–521. doi:10.1038/nsmb.3210.

Crystal structure of the prefusion surface glycoprotein of the prototypic arenavirus LCMV

Kathryn M. Hastie[#1], **Sébastien Igonet**[#1,7], **Brian M. Sullivan**[1], **Pierre Legrand**[2], **Michelle A. Zandonatti**[1], **James E. Robinson**[3], **Robert F. Garry**[4], **Félix A. Rey**[5], **Michael B. Oldstone**[1], and **Erica Ollmann Saphire**[1,6]

[1]Department of Immunology and Microbial Science, The Scripps Research Institute, La Jolla, CA, USA

[2]SOLEIL Synchrotron, Gif-sur-Yvette, France

[3]Department of Pediatrics, School of Medicine, Tulane University, New Orleans, LA, USA

[4]Department of Microbiology and Immunology, Tulane University, New Orleans, LA, USA

[5]Département de Virologie, Unité de Virologie Structurale, Institut Pasteur, Paris, France

[6]Skaggs Institute for Chemical Biology, The Scripps Research Institute, La Jolla, CA, USA

[#] These authors contributed equally to this work.

Abstract

Arenaviruses exist worldwide and can cause hemorrhagic fever and neurologic disease. A single glycoprotein is expressed on the viral surface that mediates entry into target cells. This glycoprotein, termed GPC, contains a membrane-associated signal peptide, a receptor-binding subunit termed GP1 and a fusion-mediating subunit termed GP2. Although GPC is a critical target of antibodies and vaccines, the structure of the metastable GP1-GP2 prefusion complex has remained elusive for all arenaviruses. Here we describe the crystal structure of the fully glycosylated, prefusion GP1-GP2 complex of the prototypic arenavirus LCMV at 3.5Å. This structure reveals the conformational changes that the arenavirus glycoprotein must undergo to cause fusion, and illustrates the fusion regions and potential oligomeric states.

Correspondence to: erica@scripps.edu.

[7]Current address: Calixar, Lyon, France.

Accession code and author information

Crystallographic structure factors and coordinates are deposited into the Protein Data Bank with accession number 5INE. MacPyMol, Chimera and Adobe Illustrator were used to make figures. The authors declare no conflicts of interest. This is manuscript #29106 from The Scripps Research Institute.

Author Contributions

K.M.H. built and refined the model, cloned the constructs for biochemical characterization, preformed the receptor binding experiments, analyzed the data, and wrote the manuscript; S.I. cloned the constructs for crystallization, produced and crystallized the recombinant glycoprotein ectodomains, collected diffraction data at room temperature, phased the data and determined the structure; B.M.S. grew the recombinant viruses, designed and performed the receptor binding experiments, and analyzed the data; P.L. collected diffraction data on frozen crystals and built and refined the model; M.A.Z. cloned the constructs and produced recombinant protein; J.E.R. and R.F.G generated and produced antibodies used throughout the studies; F.A.R. supervised the initial work towards structure determination; M.B.A.O designed experiments and analyzed the data; and E.O.S analyzed the data and wrote the manuscript. K.M.H and S.I contributed equally to the study. All authors commented on the manuscript.

Introduction

Arenaviruses exist worldwide, cause a tremendous disease burden, and include over 30 known pathogens divided into Old World and New World groups. The Old World arenavirus Lassa can cause hemorrhagic fever, with estimates of up to hundreds of thousands of infections and tens of thousands of deaths each year in Western Africa. Another Old World arenavirus, lymphocytic choriomeningitis virus (LCMV), exists in all populated continents with a 2-5% worldwide seroprevalence [1-7]. LCMV can cause neurologic disease and mild to lethal febrile disease in transplant recipients [7,8] and congenital birth defects and mental retardation in the fetus if acquired during pregnancy [7,9]. The disease is historically underreported, but appears to be re-emerging, especially among the immune compromised, children and pregnant women. LCMV was the first arenavirus to be isolated [10], and has illuminated much of our basic understanding of immunology and virology for decades [11-14].

All arenaviruses are pleiomorphic, enveloped virions with a four-gene, bi-segmented, ambisense RNA genome. The surface glycoprotein (GPC) is translated as a 70-80 kDa precursor protein and is translocated into the ER. There, a 58-residue stable signal peptide (SSP) is cleaved from its N terminus. Next, GPC is further proteolytically processed by site 1 protease (S1P; a.k.a. subtilisin-kexin-isozyme-1, SKI-1) to yield two subunits: the 44kDa peripheral GP1 and the 35kDa transmembrane GP2. GP1 is responsible for receptor engagement and GP2 is responsible for membrane fusion [7].

The SSP subunit of the arenavirus envelope remains associated with GP1 and GP2 on the virion surface in a tripartite complex [15,16]. SSP is important for cleavage and maturation of GPC, is an essential component of the mature viral-surface complex, associates with the transmembrane domain of GP2 [15,17-21], and may play a critical role in pH-dependent fusion of GP [16,20,22,23]. The required association of SSP with the rest of the glycoprotein on the viral surface is different from the signal peptides of class I glycoproteins such as influenza and HIV-1, which are not retained with the rest of the glycoprotein after cleavage from the precursor.

The only known receptor for LCMV is α-dystroglycan (α-DG) [24]. Interaction of LCMV with α-DG is dependent on specific glycosylation mediated by the glycosyltransferase LARGE [25-27]. The other major Old World arenavirus Lassa virus (LASV) also binds to α-DG on the cell surface [24], but additionally requires Lamp1 for infection [28]. Although New World arenaviruses of clade C similarly use α-DG as their receptor [29], pathogenic New World arenaviruses of clades A and B use a different molecule, Transferrin receptor 1 (TfR1) [29-31]. After receptor binding, all arenaviruses enter via endocytosis. Exposure of their GPC to acidic pH in the target cell endosome triggers dissociation of GP1 from GP2, and irreversible conformational changes in GP2 which drive fusion of virus and host membranes. Crystal structures of arenavirus GP2 subunits in their post-fusion conformation illustrate six-helix bundle structures typically characteristic of class I viral glycoproteins [32-34].

No structure of the prefusion form of the GP1-GP2 protomer for any member of the substantial arenavirus family has yet been described. Thus, we determined the structure of

the pre-fusion form of the surface glycoprotein of LCMV GP to 3.5Å (Table 1, Supplementary Fig. 1). This structure revealed the interactions between GP1 and GP2 and the conformational changes that the arenavirus glycoprotein must undergo to cause fusion. Further, the structure suggested that the arenavirus GP shares some features with other glycoprotein classes. This work can provide the first step in devising immunogens likely to induce neutralizing antibodies, and provides the roadmap to understand maturation, egress and entry of this extensive family of pathogens.

Structure of GP1

GP1 is a single domain structure that can be subdivided into an N-terminal β-strand, an upper "β-sheet" face and a lower "helix-loop" face (Fig. 1). The N-terminal β-strand (β1) extends away from the main body of GP1 to interact with two strands from GP2 and assemble a three-stranded, anti-parallel β–sheet (Fig. 1a). In the main body of GP1, the upper "β-sheet face" is formed by a six-stranded, anti-parallel β-sheet and contains the NxS/T sequons for the six N-glycosylation sites. Together, this array of glycans shields GP1 (Fig. 1b and Supplementary Fig. 1d). The lower, helix-loop face contains five α-helices and three extended loops.

The Old World LCMV GP1 and the New World, clade B Machupo virus (MACV) GP1[35,36] are only 20% identical in amino acid sequence and employ different cell surface receptors. The structure of MACV GP1 could not be used as a successful molecular replacement model for LCMV GP1, and so the structure was determined by heavy atom phasing. Upon structure determination, we found that the GP1s from both of these arenaviruses, as well as that of the recently determined Junin virus (JUNV) [37] have a similar core (Fig. 2a). The six-stranded β-sheet of GP1 and most of the helices on the helix-loop face are maintained between the LCMV, MACV and JUNV GP1 structures. The primary structural differences are contained in the flexible connecting loops, which comprise less than 25% of the total residues built in LCMV GP1. The structural and sequence differences were also reflected in the electrostatic surface potential whereby the β-sheet face of LCMV GP1 is acidic and the lower helix-loop face basic, while both faces are acidic in MACV GP1 (Fig. 2 c,d).

There were stark differences, however, between LCMV GP1 in this GP1-GP2 complex and the recent structure of the much more closely related LASV GP1, which was determined in isolation (without GP2)[38] (Fig. 2b and Supplementary Fig. 2). While the N- and C-termini of LCMV, MACV and JUNV GP1 are both oriented towards the GP1-GP2 interface, the termini in LASV GP1 are oriented in the opposite direction (Supplementary Fig. 2a). More significantly, the orientation of each major helix in the equivalent "helix-loop" face of LASV GP1 is nearly perpendicular to the orientation in which these helices appear in LCMV, MACV and JUNV GP1. For example, residues 126-148 in LCMV GP1 form two separate helices α1 and α2. In LASV GP1, they instead form a single, continuous helix that is rotated relative to the rest of the GP1 core by nearly 90°. Further, helix α3 in LASV GP1 is rotated ~45° relative to the position of α3 of LCMV GP1 (Supplementary Fig. 2b). As a result of these structural differences, the electrostatic surface potential of LASV GP1 is also altered considerably from that of LCMV GP1 (Fig. 2c, e).

Structure of GP2

The GP2 subunit contains the fusion regions and heptad repeats (HR) (Fig. 1c). In general, class I viral glycoproteins have a fusion peptide at the N-terminus of the fusion subunit, although some like Ebola virus, instead have a fusion loop internal to the GP2. All class II and III glycoproteins have internal fusion loops. LASV is thought to employ both an N-terminal fusion peptide (termed F1) and a fusion loop (termed F2) [39]. The amino acid sequences in F1 and F2 are nearly identical across the entire arenavirus family (Supplementary Fig. 3a, c), suggesting that the arrangement observed here might be in common among the arenaviruses. In LCMV numbering, the N-terminal fusion peptide F1 comprises residues 266-272 and the internal fusion loop F2 comprises residues 289-300.

In this crystal structure, residues of the F1 N-terminal peptide are at the dimeric interface and make both hydrophobic and hydrophilic inter-protomer contacts with loop 1 in the opposing GP1. The F1 peptide is partly helical and similar in structure to the fusion peptide of parainfluenza 5 virus F [40]. In contrast, the F2 internal loop uses an anti-parallel β strand scaffold to display a hydrophobic fusion segment at its center, similar to the fusion loops of Ebola virus GP and those of the class II and III viruses (Supplementary Fig. 4).

Comparison of the previously described post-fusion form of LCMV GP2 with the GP2 structure presented here reveals several striking differences. In the pH-induced post-fusion conformation, HR1 and HR2 each form a single helix, with the 41-residue ‘T loop’ in between. Three copies of each gather to form an antiparallel six-helix bundle (6HB) [33,41]. In the crystal structure presented here, HR1, the T loop and HR2 adopt conformations and interactions different from those in the post-fusion form (Fig. 1d). In this likely prefusion structure, HR1 is broken into four segments (HR1a, HR1b, HR1c and HR1d). HR1a, c and d form discrete helices, while HR1b adopts an extended loop structure. Here also, the T-loop of GP2 forms two anti-parallel β strands, instead of the α helix observed in the post-fusion structure. This difference suggests that GP2 conformational rearrangements occur in the T loop as well as the heptad repeat regions. The three potential glycosylation sites in GP2 are located in the T-loop, two of which are visualized here and contribute to the glycan shield on the upper surface of the GP complex (Fig. 1b). Lastly, in this likely prefusion crystal structure, HR2 forms hydrophobic contacts with the T-loop β sheet and the N-terminus of GP1. In the post-fusion structure, it instead packs against HR1 in the anti-parallel six-helix bundle (Fig. 1d).

The GP1-GP2 protomer

GP1 and GP2 are intimately associated with one another with ~5300Å^2 of surface area buried at the GP1-GP2 interface (Fig. 3a). The interface can be mapped to four primary regions: (I) the N-terminal portion of GP1 contacts HR2 of GP2; (II) β1 of GP1 assembles with the T-loop strands β10 and β11 of GP2; (III) F2 contacts β1 and the loop connecting β1 and β2 of GP1; and (IV) α4 of GP1 occupies a cleft between HR1c and HR1d in GP2 and likely anchors these helices in the pre-fusion state.

Electrostatic surface analysis of LCMV GPe revealed the β-sheet surface of GP1 is primarily acidic while both the lower helix-loop face of GP1 and the GP1-GP2 assembly sites have a largely basic surface (Fig. 3b). A deep, basic pocket is formed by the interface between α4 in GP1 and HR1d in GP2.

The dimeric interface

Expression of GPe yielded stable dimers, as determined by size exclusion chromatography in tandem with multi-angle light scattering (SEC-MALS) (Supplementary Fig. 1b, c). The asymmetric unit contains two copies of LCMV GPe in a 2-fold related antiparallel dimer covering a total of 4300 $Å^2$ buried surface (Fig. 4). The core of the interaction is a four-helix bundle created by the two copies of α2 in GP1 and the two copies of HR1c in GP2 (Fig. 4a). Also buried in the dimer interface is the GP2 fusion peptide F1, which bridges across to GP1 of the opposing protomer (Fig. 4b), forming an extensive hydrogen bond network and additional hydrophobic interactions. This arrangement of F1 is reminiscent of the flavivirus envelope protein E, in which the fusion loop is buried at the dimer interface [42-45].

To investigate potential biological significance of the dimer observed in solution and in the asymmetric unit, we made the single point mutations H136R and S143R, which lie at this interface and analyzed them biochemically (Supplementary Fig. 5a). First, we produced recombinant H136R- or S143R- bearing GPe in S2 cells and analyzed the proteins by SEC-MALS. Both H136R-GPe and S143R-GPe eluted later than WT-GPe and show a molar mass corresponding to a stoichiometry of ~1 and 1.5, respectively, demonstrating that both mutations result in defects in dimerization (Supplementary Fig 5b). We next determined whether the transmembrane GPC bearing these mutations showed similar expression and processing as WT GPC when transiently expressed in vitro. Although both mutations expressed at near-WT levels, their GPC appeared to be largely unprocessed (Supplementary Fig 5c). We also attempted to rescue recombinant viruses bearing each mutation. H136R-bearing viruses rescued to similar titers as WT HPI viruses while S143R-bearing viruses rescued poorly (Supplementary Table 1). S143R is located in α2 of GP1 and is in the center of the dimeric interface while H136R resides on the outer edge of the interface (Fig. 4, Supplementary Fig. 5a).

Dystroglycan binding

Strains of LCMV can be divided into two groups: those that have high affinity for α-dystroglycan (αDG) and cause persistent infection, and those that have 2-2.5 logs lower affinity for αDG and cause a readily clearable infection [46-50] Serine at position 153 and leucine at position 260 confer high-affinity αDG binding and persistent infection [49,51,52]. These residues can now be visualized in this structure; both are located in the lower, helix-loop face of GP1 (Supplementary Fig. 2b).

The strain of LCMV crystallized here, WE HPI, encodes both S153 and L260, yet binds to αDG poorly (Fig. 5), suggesting that additional residues also contribute to αDG affinity and interaction. Alignment of this low-affinity WE HPI sequence with that of the similarly low-affinity WE2.2 and conversely high-affinity WE54 pinpointed two other positions, residues

155 and 211, where low- and high-affinity strains differ (Supplementary Fig. 3a). We mutated each of these positions in WE HPI to the high-affinity WE54 sequence (H155Y and A211T) and grew recombinant viruses. Both H155Y and A211T-bearing viruses grew to similar titers, but only HPI viruses bearing H155Y bound to αDG with high affinity (Fig. 5a, b). Further, only H155Y-bearing virus and not WT HPI virus showed reduced infectivity in the presence of soluble αDG (Fig. 5c). The converse mutation when put into WE54 (Y155H) resulted in a loss of its high-affinity binding to αDG and loss of infectivity reduction in the presence of soluble αDG (Fig. 5b, c). Thus, in addition to the historically known residues S153 and L260, Y155 is also required for high-affinity binding to αDG. Notably, infectivity of the low-affinity viruses WT HPI and WE54 Y155H was not affected by the presence of soluble αDG. Soluble αDG only reduces infectivity of the high-affinity strains, suggesting that these strains interact specifically with αDG, and that low-affinity strains use as as-yet-unidentified receptor.

We next sought to determine if residues other than S153, Y155 and L260 could potentially be involved in binding αDG by high-affinity viruses. We made recombinant viruses carrying single point mutations throughout the upper β-sheet surface and the basic, lower loop face of LCMV GPC and analyzed them for soluble α-DG competition. In the lower loop face, we specifically targeted basic residues that could interact with the acidic αDG sugar [25]. We also included H136R to determine if its interface may be involved in αDG binding. S143R, also at the dimer interface was not included, as it does not rescue analyzable viruses.

All recombinant viruses were made in the H155Y background to enable analysis of specific binding to αDG. Wild-type HPI was used as a control for poor DG binding. Seven of the 16 mutant viruses could be rescued to titers high enough for analysis (Fig. 6a, Supplementary Table 1). The infectivity of viruses bearing GPC-H155Y and the additional single point mutations H136R (located at the dimeric interface) or R190A (located on the lower basic loop face), was unaffected by preincubation with soluble αDG, suggesting these viruses do not bind to αDG and instead enter via another receptor (Fig. 6b). In contrast, viruses bearing GPC-H155Y alone, or GPC-H155Y plus any other point mutation on the β-sheet face or R185A (loop face), showed a 2-3 fold decrease in infection when preincubated with αDG as compared to PBS. These results indicated that in general, the high-affinity H155Y-bearing viruses did use αDG as their primary receptor in this system. In contrast, H155Y H136R and H155Y R190A viruses did not bind αDG well, even in the H155Y background, and must instead use an alternate receptor. H136 and R190 appeared important for DG affinity.

Pathogenic New World arenaviruses use Transferrin receptor 1 (TfR1) [31] to enter cells. The crystal structure of MACV GP1 in complex with TfR1 demonstrates that receptor binding occurs on the β-sheet face of GP1 and that the GP1 subunit is necessary and sufficient for receptor engagement [35]. To investigate the subunit requirements of receptor binding for LCMV, we analyzed binding of αDG to either full-length LCMV GPC or its GP1 subunit alone from the high-affinity H155Y mutant, by immunoprecipitation of αDG from cells over-expressing the LARGE glycosyltransferase necessary for correct modification of the receptor. In this context, only H155Y GPC, and not H155Y GP1, was able to precipitate αDG (Fig. 5d). Similar results were recently reported for LASV, whereby only full-length GPC, and not GP1, successfully pulls down αDG [28,38]. These results suggest that for Old

World arenaviruses, either avidity, or a quaternary assembly of GP1, provided only in the context of the GPC, is necessary for αDG engagement.

LAMP1 binding

Recent work by Jae, et al [28] demonstrates that LASV requires interaction with LAMP1 for infection and that this interaction occurs only at low pH. Additional studies by Cohen-Dvashi, et al., identify a histidine triad in LASV necessary for LAMP1 binding. Even though this triad (H97, H98 and H238 in LCMV numbering), and the β-sheet face that contains it are conserved between LASV and LCMV (Supplementary Figs. 2 and 3a, b), LAMP1 is not required for infection by LCMV Armstrong [28].

LASV binds to αDG with higher affinity than LCMV Armstrong [24]. We postulated that dependence on LAMP1 might correlate with αDG use. We compared two strains that bind αDG with high affinity (Cl. 13 and WE HPI H155Y) and two strains that bind αDG with low affinity (Armstrong and WT WE HPI) in differences in infection efficiency of BHK cells versus LAMP1 knock-out cells. All four strains entered both cell lines with equal efficiency, demonstrating that regardless of the affinity for DG, LAMP1 does not act as an essential factor for LCMV infection (Figure 6c). Curiously, recombinant viruses with GPCs bearing H98A or H238A mutations, two of three triad residues necessary for LASV GP1–LAMP1 interaction, failed to rescue or rescued very poorly, respectively. H98 and H238 in LCMV may be involved in the overall stability of GPC or in binding to an as-yet-unknown receptor for LCMV (Supplementary Table 1).

Fitting of the LCMV GP protomer into LASV GPC spike density

Crystal structures of post-fusion arenavirus GP2 are trimeric [33,41], as are tomograms of viral-surface LASV GPC [53]. The dimers of the asymmetric unit trimerize in crystals via interactions of the GP1 N terminus to F2 of a neighboring protomer, HR2 to F1 of a neighboring protomer, and assembly of the GP2 T-loops in the center of the trimer axis. However, in this arrangement, there is no three-helix core in the GP2 ectodomain, as found in other type I glycoproteins, and the buried surface area at the trimer interface is modest. Instead, we fit three single copies of the prefusion LCMV GP protomer into the LASV GPC tomographic density allowing all glycans to point outward (Fig. 7). Curiously, if glycans point outward, residues 153, 155, and 190 of basic helix-loop face, which are important for αDG interaction, point inward, towards the three-fold axis. This arrangement suggests that the acidic sugar attached to αDG binds down into the trimer center, a conformational rearrangement from this trimer is required for binding αDG, or the importance of these residues lies in maintenance of the right quaternary assembly for αDG interaction.

Discussion

Here we provide the crystal structure of the GP1-GP2 protomer of LCMV, the prototypic virus in the family *Arenaviridae*. The GP2 in this complex exists in a substantially different conformation than observed in the post-fusion six-helix bundle structures of GP2 from LCMV [33] or the New World Venezuelan hemorrhagic fever virus [41]. We find evidence for

structural rearrangements of both the heptad repeats and the T-loop that likely occur during fusion. Further, the conformation of GP2 observed here has intimate association with GP1, and both F1 and F2 fusion sequences, now visualized, are buried at oligomeric interfaces, suggesting that this structure represents the prefusion form of the GP protomer. The GP2 subunits of the arenaviruses are 75% similar by sequence, and this Old World GP1 is structurally similar to that of the New World MACV and JUNV. Thus, the arrangement of the GP1-GP2 assembly presented here is likely shared among the entire arenavirus family.

The presence of a six-helix bundle in the pH-induced, post-fusion conformation demonstrates that LCMV GP forms a trimer to mediate membrane fusion [32,33,41]. However, the existence of LCMV GPe as a dimer in solution and in crystals and the extensive buried surface of the dimer interface (5,300 $Å^2$) suggests that a similar interface may exist at some point in the virus life cycle. Dimers of GP have been previously observed in analysis of protein-protein interactions in LCMV particles [54]. The mutations H136R or S143R inhibit dimer formation and prevent proper processing of GPC in transient transfection studies. Further, the S143R mutation results in non-rescuable virus. The H136R mutation does result in rescuable virus, but this virus is unable to bind to the αDG receptor. Thus, residues at this observed interface are directly or indirectly critical for high-affinity αDG engagement.

In the GP structure presented here, both the hydrophobic fusion loop and fusion peptide are buried at a dimer interface. Curiously, this arrangement is unlike known class I fusion proteins, and instead, more like the class II flavivirus envelope protein. The flavivirus envelope protein adopts trimer-to-dimer and dimer-to-trimer rearrangements in maturation and fusion and also possesses a transmembrane subunit, termed M, which remains associated with E on the viral surface and plays a role in its oligomeric transitions. Thus, M may be functionally similar to the required transmembrane SSP subunit of the arenaviruses (as reviewed in 55). In the LCMV dimer, the two GPs in the asymmetric unit interact in an anti-parallel fashion, like those of flavivirus E. In this organization, the 16-residue MPER region could allow both GP1-GP2 protomers to be anchored into the endoplasmic reticulum or viral membrane. The arenaviruses, with their positive-sense GP coding, required SSP subunit, unexpected oligomeric interface, and atypical fusion structure have a unique architecture with similarities to and differences from other viral classes observed before.

We used the crystal structure of this prefusion GP protomer to identify residues critical for binding of the only known receptor for LCMV, αDG. The exact role, however, of each of the five residues now identified, 136, 153, 155 and 190, remains to be elucidated. 153, 155 and 190 are located in or around Loop1, but 136 and 260 are each located 20-25Å away in opposite directions from one another (Fig. 6a). Binding of a single sugar likely does not occur over a 50Å-wide surface. All of these residues are contained in the GP1 subunit. However, for both LASV [38] and LCMV (this study), full-length GPC, and not the GP1 alone, are required for αDG engagement. These findings suggest that complete GPC may be required because it builds a particular quaternary assembly or GP1 orientation for αDG binding.

We find that LCMV GP1 is unexpectedly much more similar in structure to MACV and JUNV GP1 (20% identical in sequence) than it is LASV GP1 (63% identical in sequence).

One of the few structural elements in common between LASV and LCMV is Loop1, which contains residues critical for αDG interaction. Elsewhere in GP1, the significant structural differences between LASV and LCMV cannot be easily explained by sequence, the presence or absence of GP2, nor the pH of crystallization (MACV and LASV GP1 were crystallized at pH 5.5 and 5, respectively, while JUNV GP1 and LCMV GP were crystallized at pH 8.0 and 7.5, respectively). It is known that GP2 undergoes conformational change at low pH; perhaps GP1 of LASV has a pH-induced conformational change as well, and this conformational change is related to dependence on LAMP1 for entry. Alternatively, there may be plasticity in GP1 in the absence of GP2.

In contrast to GP1, GP2 is highly conserved in sequence among Old and New World arenaviruses alike. The work presented here reveals the probable prefusion conformation of arenavirus GP2, the conformation of its fusion sequences and the sites and modes of interaction of prefusion GP2 with GP1. These structural interactions and potential oligomeric assemblies likely illuminate how other arenavirus glycoproteins function as well, and open lines of inquiry into maturation, assembly and entry of this unique and very large family of human pathogens.

Online Methods

Expression and purification

The soluble ectodomain (residues 1-438, GPe), or the ectodomain fused at the GP2 C terminus to the trimerization motif of T4 fibritin (GPeFib), each belonging to the LCMV GP strain WE HPI, were cloned into the pMTpuro vector for stable expression in *Drosophila* S2 cells (Invitrogen, not tested for mycoplasma contamination) (Supplementary Fig. 1a). Cells were grown in shaker flasks to a density of 6-8×10^6 cells/mL and expression was induced with 500μM $CuSO_4$. Expression was carried out for 6-8 days and protein was purified from the supernatant via streptactin-affinity chromatography, followed by size-exclusion chromatography (SEC) using a S200 16/60 column. Unexpectedly, the soluble ectodomain yielded stable dimers, as determined by size exclusion chromatography in tandem with multi-angle light scattering (SEC-MALS) (Supplementary Fig. 1b). While the native S1P cleavage site (RRLA) was not altered, the S1P expressed by S2 cells did not act upon the GP and thus all GP purified was in an unprocessed form. However, GPeFib was further screened with limited proteolysis via 1:1000 (w/w) of trypsin (GPeFibTryp). Trypsinization cleaved the peptide bond between GP1 and GP2 and based on the loss of ~7kDa and loss of reactivity to an anti-strep antibody, likely also removed the fibritin motif and double strep tag (Supplementary Fig. 1c).

Crystallization, Data Collection, and Structure Determination

Initial crystal screening of GPe and GPeFib was carried out using sparse matrix screens and an Oryx crystallization robot (Douglas Instruments). Only GPe produced initial hits, which were further optimized in larger-scale formats and conditions refined. Final crystallization conditions of 0.1M Hepes pH 7.5, 20% PEG 2k and 0.2M lithium sulfate produced cubic-type crystals after 2-3 months without seeding and within 1-2 weeks with seeding. GPeFib did not produce crystals on its own or when seeded with GPe crystals. However, when

treated with trypsin and seeded with GPe crystals, GPeFibTryp crystallized in the same condition and with the same morphology as GPe.

For several years, despite extensive optimization of cryo conditions and freezing techniques, data collected from GPe crystals at room temperature was consistently superior. Thus, to achieve a complete data set, images from three independent crystals were collected at SSRL beamline 11-1 and data processed with XDS [57]. Molecular replacement using the available structures of Machupo virus GP1 [35,36], its core or Cα trace, or any portion of the post-fusion LCMV GP2 [33] was unsuccessful. Phases were instead obtained by soaking GPe crystals with TaBr, which enabled structure determination by SIRAS (Table 1). Heavy atom sites were identified using autoSHARP [58]. An initial Cα backbone trace was built using Buccaneer [59,60] and the necessary rebuilding and refinement preformed using Coot [61] and Phenix [62], respectively.

Native crystals of GPeFibTryp diffracted to 3.5Å when frozen in ParatoneN Oil (Hampton Research) and data were collected at SOLEIL Proxima 1. Data were processed using XDS and merged prior to scaling. Molecular replacement was performed with Phaser using the model obtained from the GPe TaBr-phased data. Rebuilding and refinement of this data were performed using Coot [61], Phenix [62] and Buster TnT [63]. The unit cell, space group and models of GPe and GPeFibTryp are essentially identical.

Positions of the sulfur-containing cysteine and methionine residues in the model were confirmed via a Sulfur SAD experiment, using highly redundant data collected to 4Å from a single, frozen crystal of GPeFibTryp at SOLEIL Proxima 1. The register was further confirmed by identification of N-linked glycan sites at NXS/T sequons and large aromatic residues in the GP model (Supplementary Fig. 1d).

Two copies of the GP1-GP2 protomer (protomers A and B) are contained in the asymmetric unit. The final model contains residues 63 to 427 in monomer A and residues 63 to 424 in monomer B. Four short sections of GP1 are disordered in both protomers (residues 59-62, 175-183, 214-218, and 262-265. The latter is at the GP1-GP2 junction). An additional disordered region occurs in protomer B at residues 275-282 in GP2. The final model has an R/R_{free} of 0.2106/0.2308 with an overall score of 2.08 and clash score of 2.36 and with 2% Ramachandran outliers (one residue in each chain) and 4% rotomer outliers as calculated by Molprobity. Full data statistics can be found in Table 1.

SEC-MALS

Approximately 250ug of GP was separated on a Superose6 column (GE Healthcare) using an AKTA FPLC system (GE Healthcare). Size exclusion chromatography (SEC) was coupled inline with the following calibrated detectors: 1) a MiniDawn Treos multi-angle light scattering (MALS) detector (Wyatt Corporation); and 2) an Optilab T-reX refractive index (RI) detector (Wyatt Corporation). The Astra VI software (Wyatt Corporation) was used to combine these measurements and allow the absolute molar mass of the eluting glycoprotein, as well as the individual contributions from the protein and glycan components, to be determined [64,65].

Plasmids

Full-length LCMV WE HPI GPC, derived from a synthetic, codon-optimized gene, was cloned into the phCMV vector for transfection into 293T cells (ATCC CRL-3216, tested for mycoplasma contamination). Mutations were introduced using site-directed mutagenesis and positive clones confirmed by sequencing. To generate plasmids for the expression of GP1 alone, residues 59-262 of the GPC were cloned into a phCMV vector that was engineered to express the IgK secretion signal and N-terminal HA tag. Wild-type and mutant GPCs were sub-cloned into the pT7-S(+)HR vector [66] used for the generation of recombinant viruses and re-sequenced to confirm no additional mutations were introduced.

Virus Rescue

Recombinant viruses were generated as previously described [66].

VOPBA analysis of receptor binding

A soluble dystroglycan fragment fused to the Fc region of human IgG1 (DGFc4) was expressed and purified as previously described [67,68]. Briefly, DGFc4 was blotted onto nitrocellulose membranes in decreasing concentrations and incubated with purified recombinant LCMV. Bound viral particles were detected by dot blot using the anti-GP1 antibody WE36.1 [69] and the anti-GP-2 antibody WE33.6 [69] followed by anti-mouse IgG-HRP.

ELISA analysis of receptor binding

ELISAs measuring virus-receptor binding was performed as previously described [67,68]. Briefy, 2×10^6 pfu/well of each virus was coated to ELISA plates. After blocking with BSA, DGFc4 was bound to viruses and detected using a mouse anti-human IgG-Fc followed by goat anti-mouse IgG-HRP antibody.

DG pull-down analysis

293T cells were transfected with wild-type or H155Y GPC or H155Y GP1 plasmids. 72 hours post-transfection, the supernatant of GP1 transfected cells was clarified and secreted GP1 captured with anti-HA agarose beads (Thermo Scientific) for 1hr at 4C. For both GPC and GP1 transfections, cells were washed with PBS and lysed with PBS supplemented with 1% NP-40 and protease inhibitor cocktail. Clarified lysates were bound to anti-HA beads for 1hour at 4C. Following capture of GP1 or GPC, beads were washed twice with PBS/1%NP-40. An equal amount of lysate from 293T cells stably expressing the LARGE glycosyltransferase was incubated with captured GP1 or GPC for 1hr at 4C. Beads were washed three times with PBS/1% NP-40 and bound proteins eluted with 1xSDS loading buffer. Samples were separated by SDS-PAGE and transferred to PDVF membranes. DG was detected with the monoconal IIH6 antibody (Santa Cruz Biotechnology, validation provided on manufacturer website) followed by anti-mouse IgM-HRP. GP1 was detected with the anti-WE GP1 antibody KL25 (gift of M. Buchmeier, University of California, Irvine[70]) followed by anti-mouse IgG-HRP.

DG competition/infectivity studies

DGFc4 was incubated with virus at a MOI of 1 for 1 hour at 37°C in either a series of dilutions of DGFc4 or with 30-100pmol of DGFc4. The mixture was transferred to BHK-21 cells (ATCC CCL-10, tested for mycoplasma contamination) and incubated for an additional hour. Cells were washed three times in PBS. Supernatants collected 24hr post-infection and quantified by fluorescence focus assay with an Alexa Fluor 488 conjugated LCMV anti-NP (clone VL-4) antibody [71].

Infectivity assays with LCMV

LAMP1 knock-out cells (gift of S. Whelan, Harvard Medical School) were grown in IMDM-GlutaMAX media supplemented with 10% FBS and 100g/mL penicillin/streptomycin. BHK-21 cells were grown in DMEM supplemented with 10% FBS, 100g/mL penicillin/streptomycin, 2mM L-glutamine, 7% tryptose phosphate broth solution (Sigma), and 0.56% glucose (wt/vol). LAMP1 knock-out cells and BHK control cells were collected with non-enzymatic cell dissociation solution (Sigma) and incubated with LCMV at a MOI of 1 at 37°C for 1 hour. Cells were washed twice with PBS and plated in their respective media. Cells were collected 24 hours post-infection, fixed, permeabilized (BD cytofix/cytoperm kit), and stained with Alexa Fluor 488 conjugated LCMV anti-NP (clone VL-4 [71]) antibody. Cells were washed and analyzed by flow cytometry (LSR II, Becton Dickinson) and data subsequently analyzed with FlowJo software (FlowJo, LLC).

Supplementary Material

Refer to Web version on PubMed Central for supplementary material.

Acknowledgements

The authors wish to acknowledge the Viral Hemorrhagic Fever Research Consortium and US National Institutes of Health grant 1U19AI109762-01 (E.O.S., J.E.R. and R.F.G), US National Institutes of Health grant R21 AI116112 (EOS), an Investigators in Pathogenesis of Infectious Diseases award from the Burroughs Wellcome Fund (EOS), and US National Institutes of Health grants AI009484 (MBAO) and A1099699 (MBAO) for funding; Xiaoping Dai for assistance with data processing; M. Buchmeier (University of California, Irvine) for the anti-LCMV GP1 (KL25) antibody; and Beamlines 11-1, 12-1 and 12-2 of the Stanford Synchrotron Radiation Lightsource (Palo Alto, CA), 5.0.2, 5.0.3 and 8.2.2 of the Advanced Light Source (Berkeley, CA), 19-ID, 23-ID-B and 23-ID-D of the Advanced Photon Source (Argonne, IL) and SOLEIL Proxima 1 (Gif-sur-Yvette, France) for data collection; and C. Corbaci for assistance in creating figures.

References

1. Stephensen CB, et al. Prevalence of serum antibodies against lymphocytic choriomeningitis virus in selected populations from two U.S. cities. J Med Virol. 1992; 38:27–31. [PubMed: 1402829]
2. Childs JE, et al. Human-rodent contact and infection with lymphocytic choriomeningitis and Seoul viruses in an inner-city population. Am J Trop Med Hyg. 1991; 44:117–21. [PubMed: 1672798]
3. Ambrosio AM, Feuillade MR, Gamboa GS, Maiztegui JI. Prevalence of lymphocytic choriomeningitis virus infection in a human population of Argentina. Am J Trop Med Hyg. 1994; 50:381–6. [PubMed: 8147496]
4. Marrie TJ, Saron MF. Seroprevalence of lymphocytic choriomeningitis virus in Nova Scotia. Am J Trop Med Hyg. 1998; 58:47–9. [PubMed: 9452291]
5. Lledo L, Gegundez MI, Saz JV, Bahamontes N, Beltran M. Lymphocytic choriomeningitis virus infection in a province of Spain: analysis of sera from the general population and wild rodents. J Med Virol. 2003; 70:273–5. [PubMed: 12696116]

6. Riera L, et al. Serological study of the lymphochoriomeningitis virus (LCMV) in an inner city of Argentina. J Med Virol. 2005; 76:285–9. [PubMed: 15834871]
7. Buchmeier, M.; de la Torre, JC.; Peters, CJ. Arenaviridae: the viruses and their replication. Lippincott-Raven; Philadelphia: 2007.
8. Fischer SA, et al. Transmission of lymphocytic choriomeningitis virus by organ transplantation. N Engl J Med. 2006; 354:2235–49. [PubMed: 16723615]
9. Jamieson DJ, Kourtis AP, Bell M, Rasmussen SA. Lymphocytic choriomeningitis virus: an emerging obstetric pathogen? Am J Obstet Gynecol. 2006; 194:1532–6. [PubMed: 16731068]
10. Armstrong, C.a.R.D.L. Experimental lymphocytic choriomeningitis of monkeys and mice produced by a virus encountered in studies of the 1933 St. Louis epidemic. Publ Health Rep. 1934; 49
11. Oldstone MB. Lessons learned and concepts formed from study of the pathogenesis of the two negative-strand viruses lymphocytic choriomeningitis and influenza. Proc Natl Acad Sci U S A. 2013; 110:4180–3. [PubMed: 23341590]
12. Pauken KE, Wherry EJ. Overcoming T cell exhaustion in infection and cancer. Trends Immunol. 2015
13. Zinkernagel RM. Lymphocytic choriomeningitis virus and immunology. Curr Top Microbiol Immunol. 2002; 263:1–5. [PubMed: 11987811]
14. Gourley TS, Wherry EJ, Masopust D, Ahmed R. Generation and maintenance of immunological memory. Semin Immunol. 2004; 16:323–33. [PubMed: 15528077]
15. Eichler R, et al. Identification of Lassa virus glycoprotein signal peptide as a transacting maturation factor. EMBO Rep. 2003; 4:1084–8. [PubMed: 14555961]
16. York J, Romanowski V, Lu M, Nunberg JH. The signal peptide of the Junin arenavirus envelope glycoprotein is myristoylated and forms an essential subunit of the mature G1-G2 complex. Journal of Virology. 2004; 78:10783–92. [PubMed: 15367645]
17. Eichler R, Lenz O, Strecker T, Garten W. Signal peptide of Lassa virus glycoprotein GP-C exhibits an unusual length. FEBS Lett. 2003; 538:203–6. [PubMed: 12633879]
18. Froeschke M, Basler M, Groettrup M, Dobberstein B. Long-lived signal peptide of lymphocytic choriomeningitis virus glycoprotein pGP-C. Journal of Biological Chemistry. 2003; 278:41914–20. [PubMed: 12917426]
19. Kunz S, Edelmann KH, de la Torre JC, Gorney R, Oldstone MB. Mechanisms for lymphocytic choriomeningitis virus glycoprotein cleavage, transport, and incorporation into virions. Virology. 2003; 314:168–78. [PubMed: 14517070]
20. Saunders AA, et al. Mapping the landscape of the lymphocytic choriomeningitis virus stable signal peptide reveals novel functional domains. Journal of Virology. 2007; 81:5649–57. [PubMed: 17376927]
21. Schrempf S, Froeschke M, Giroglou T, von Laer D, Dobberstein B. Signal peptide requirements for lymphocytic choriomeningitis virus glycoprotein C maturation and virus infectivity. J Virol. 2007; 81:12515–24. [PubMed: 17804515]
22. York J, Nunberg JH. Role of the stable signal peptide of Junin arenavirus envelope glycoprotein in pH-dependent membrane fusion. Journal of Virology. 2006; 80:7775–80. [PubMed: 16840359]
23. York J, Nunberg JH. Distinct requirements for signal peptidase processing and function in the stable signal peptide subunit of the Junin virus envelope glycoprotein. Virology. 2007; 359:72–81. [PubMed: 17045626]
24. Cao W, et al. Identification of alpha-dystroglycan as a receptor for lymphocytic choriomeningitis virus and Lassa fever virus. Science. 1998; 282:2079–81. [PubMed: 9851928]
25. Inamori K, et al. Dystroglycan function requires xylosyl- and glucuronyltransferase activities of LARGE. Science. 2012; 335:93–6. [PubMed: 22223806]
26. Kanagawa M, et al. Molecular recognition by LARGE is essential for expression of functional dystroglycan. Cell. 2004; 117:953–64. [PubMed: 15210115]
27. Kunz S, et al. Posttranslational modification of alpha-dystroglycan, the cellular receptor for arenaviruses, by the glycosyltransferase LARGE is critical for virus binding. J Virol. 2005; 79:14282–96. [PubMed: 16254363]

28. Jae LT RM, Herbert AS, Kuehne AI, Wirchnianski AS, Soh TK, Stubbs SH, Janssen H, Damme M, Saftig P, Whelan SP, Dye JM, Brummelkamp TR. Lassa virus entry requires a trigger-induced receptor switch. Science. 2014; 344:1506–10. [PubMed: 24970085]
29. Spiropoulou CF, Kunz S, Rollin PE, Campbell KP, Oldstone MB. New World arenavirus clade C, but not clade A and B viruses, utilizes alpha-dystroglycan as its major receptor. Journal of Virology. 2002; 76:5140–6. [PubMed: 11967329]
30. Flanagan ML, et al. New world clade B arenaviruses can use transferrin receptor 1 (TfR1)-dependent and -independent entry pathways, and glycoproteins from human pathogenic strains are associated with the use of TfR1. J Virol. 2008; 82:938–48. [PubMed: 18003730]
31. Radoshitzky SR, et al. Transferrin receptor 1 is a cellular receptor for New World haemorrhagic fever arenaviruses. Nature. 2007; 446:92–6. [PubMed: 17287727]
32. Eschli B, et al. Identification of an N-terminal trimeric coiled-coil core within arenavirus glycoprotein 2 permits assignment to class I viral fusion proteins. J Virol. 2006; 80:5897–907. [PubMed: 16731928]
33. Igonet S, et al. X-ray structure of the arenavirus glycoprotein GP2 in its postfusion hairpin conformation. Proceedings of the National Academy of Sciences USA. 2011; 108:19967–72.
34. Parsy ML, Harlos K, Huiskonen JT, Bowden TA. Crystal structure of Venezuelan hemorrhagic fever virus fusion glycoprotein reveals a class 1 postfusion architecture with extensive glycosylation. J Virol. 2013; 87:13070–5. [PubMed: 24049182]
35. Abraham J, Corbett KD, Farzan M, Choe H, Harrison SC. Structural basis for receptor recognition by New World hemorrhagic fever arenaviruses. Nature Structural and Molecular Biology. 2010; 17:438–44.
36. Bowden TA, et al. Unusual molecular architecture of the machupo virus attachment glycoprotein. Journal of Virology. 2009; 83:8259–65. [PubMed: 19494008]
37. Mahmutovic S, et al. Molecular Basis for Antibody-Mediated Neutralization of New World Hemorrhagic Fever Mammarenaviruses. Cell Host Microbe. 2015; 18:705–13. [PubMed: 26651946]
38. Cohen-Dvashi H, Cohen N, Israeli H, Diskin R. Molecular Mechanism for LAMP1 Recognition by Lassa Virus. J Virol. 2015; 89:7584–92. [PubMed: 25972533]
39. Klewitz C, Klenk HD, ter Meulen J. Amino acids from both N-terminal hydrophobic regions of the Lassa virus envelope glycoprotein GP-2 are critical for pH-dependent membrane fusion and infectivity. J Gen Virol. 2007; 88:2320–8. [PubMed: 17622638]
40. Welch BD, et al. Structure of the cleavage-activated prefusion form of the parainfluenza virus 5 fusion protein. Proc Natl Acad Sci U S A. 2012; 109:16672–7. [PubMed: 23012473]
41. Parsy ML, Harlos K, Huiskonen JT, Bowden TA. Crystal structure of Venezuelan hemorrhagic fever virus fusion glycoprotein reveals a class 1 postfusion architecture with extensive glycosylation. Journal of Virology. 2013
42. Rey FA, Heinz FX, Mandl C, Kunz C, Harrison SC. The envelope glycoprotein from tick-borne encephalitis virus at 2 A resolution. Nature. 1995; 375:291–8. [PubMed: 7753193]
43. Kanai R, et al. Crystal structure of west nile virus envelope glycoprotein reveals viral surface epitopes. J Virol. 2006; 80:11000–8. [PubMed: 16943291]
44. Modis Y, Ogata S, Clements D, Harrison SC. A ligand-binding pocket in the dengue virus envelope glycoprotein. Proc Natl Acad Sci U S A. 2003; 100:6986–91. [PubMed: 12759475]
45. Modis Y, Ogata S, Clements D, Harrison SC. Variable surface epitopes in the crystal structure of dengue virus type 3 envelope glycoprotein. J Virol. 2005; 79:1223–31. [PubMed: 15613349]
46. Kunz S, Sevilla N, Rojek JM, Oldstone MB. Use of alternative receptors different than alpha-dystroglycan by selected isolates of lymphocytic choriomeningitis virus. Virology. 2004; 325:432–45. [PubMed: 15246281]
47. Oldstone MB, Campbell KP. Decoding arenavirus pathogenesis: essential roles for alpha-dystroglycan-virus interactions and the immune response. Virology. 2011; 411:170–9. [PubMed: 21185048]
48. Oldstone MBA. Biology and Pathogenesis of Lymphocytic Choriomeningitis Virus Infection. Arenaviruses II. Curr Top Microbiol Immunol. 2002; 263:83–117. [PubMed: 11987822]

49. Sevilla N, et al. Immunosuppression and resultant viral persistence by specific viral targeting of dendritic cells. J Exp Med. 2000; 192:1249–60. [PubMed: 11067874]
50. Sullivan BM, et al. Point mutation in the glycoprotein of lymphocytic choriomeningitis virus is necessary for receptor binding, dendritic cell infection, and long-term persistence. Proc Natl Acad Sci U S A. 2011; 108:2969–74. [PubMed: 21270335]
51. Smelt SC, et al. Differences in affinity of binding of lymphocytic choriomeningitis virus strains to the cellular receptor alpha-dystroglycan correlate with viral tropism and disease kinetics. J Virol. 2001; 75:448–57. [PubMed: 11119613]
52. Teng MN, Borrow P, Oldstone MB, de la Torre JC. A single amino acid change in the glycoprotein of lymphocytic choriomeningitis virus is associated with the ability to cause growth hormone deficiency syndrome. J Virol. 1996; 70:8438–43. [PubMed: 8970965]
53. Li S, et al. Acidic pH-Induced Conformations and LAMP1 Binding of the Lassa Virus Glycoprotein Spike. PLoS Pathog. 2016; 12:e1005418. [PubMed: 26849049]
54. Burns JW, Buchmeier MJ. Protein-protein interactions in lymphocytic choriomeningitis virus. Virology. 1991; 183:620–9. [PubMed: 1853564]
55. Mukhopadhyay S, Kuhn RJ, Rossmann MG. A structural perspective of the flavivirus life cycle. Nat Rev Microbiol. 2005; 3:13–22. [PubMed: 15608696]
56. Baker NA, Sept D, Joseph S, Holst MJ, McCammon JA. Electrostatics of nanosystems: application to microtubules and the ribosome. Proc Natl Acad Sci U S A. 2001; 98:10037–41. [PubMed: 11517324]
57. Kabsch W. Xds. Acta Crystallogr D Biol Crystallogr. 2010; 66:125–32. [PubMed: 20124692]
58. Vonrhein C, Blanc E, Roversi P, Bricogne G. Automated structure solution with autoSHARP. Methods Mol Biol. 2007; 364:215–30. [PubMed: 17172768]
59. Cowtan K. The Buccaneer software for automated model building. 1. Tracing protein chains. Acta Crystallographica. 2006; 62:1002–11. [PubMed: 16929101]
60. Cowtan K. Completion of autobuilt protein models using a database of protein fragments. Acta Crystallographica. 2012; 68:328–35. [PubMed: 22505253]
61. Emsley P, Cowtan K. Coot: model-building tools for molecular graphics. Acta Crystallogr D Biol Crystallogr. 2004; 60:2126–32. [PubMed: 15572765]
62. Adams PD, et al. PHENIX: a comprehensive Python-based system for macromolecular structure solution. Acta Crystallogr D Biol Crystallogr. 2010; 66:213–21. [PubMed: 20124702]
63. Bricogne, G., et al. BUSTER. 2.8.0 edn. Global Phasing, Ltd.; Cambridge, United Kingdom: 2009.
64. Wen J, Arakawa T, Philo JS. Size-exclusion chromatography with on-line lightscattering, absorbance, and refractive index detectors for studying proteins and their interactions. Anal Biochem. 1996; 240:155–66. [PubMed: 8811899]
65. Folta-Stogniew E. Oligomeric states of proteins determined by size-exclusion chromatography coupled with light scattering, absorbance, and refractive index detectors. Methods Mol Biol. 2006; 328:97–112. [PubMed: 16785643]
66. Sanchez AB, de la Torre JC. Rescue of the prototypic Arenavirus LCMV entirely from plasmid. Virology. 2006; 350:370–80. [PubMed: 16476461]
67. Kunz S, Calder L, Oldstone MB. Electron microscopy of an alpha-dystroglycan fragment containing receptor sites for lymphocytic choriomeningitis virus and laminin, and use of the receptoid body as a reagent to neutralize virus. Virology. 2004; 325:207–15. [PubMed: 15246261]
68. Kunz S, Sevilla N, McGavern DB, Campbell KP, Oldstone MB. Molecular analysis of the interaction of LCMV with its cellular receptor [alpha]-dystroglycan. J Cell Biol. 2001; 155:301–10. [PubMed: 11604425]
69. Parekh BS, Buchmeier MJ. Proteins of lymphocytic choriomeningitis virus: antigenic topography of the viral glycoproteins. Virology. 1986; 153:168–78. [PubMed: 2426862]
70. Bruns M, Cihak J, Muller G, Lehmann-Grube F. Lymphocytic choriomeningitis virus. VI. Isolation of a glycoprotein mediating neutralization. Virology. 1983; 130:247–51. [PubMed: 6636539]
71. Battegay M, et al. Quantification of lymphocytic choriomeningitis virus with an immunological focus assay in 24- or 96-well plates. J Virol Methods. 1991; 33:191–8. [PubMed: 1939506]

One Sentence Summary

The structure of the arenavirus glycoprotein complex reveals the arrangement of GP1 and GP2 subunits prior to membrane fusion.

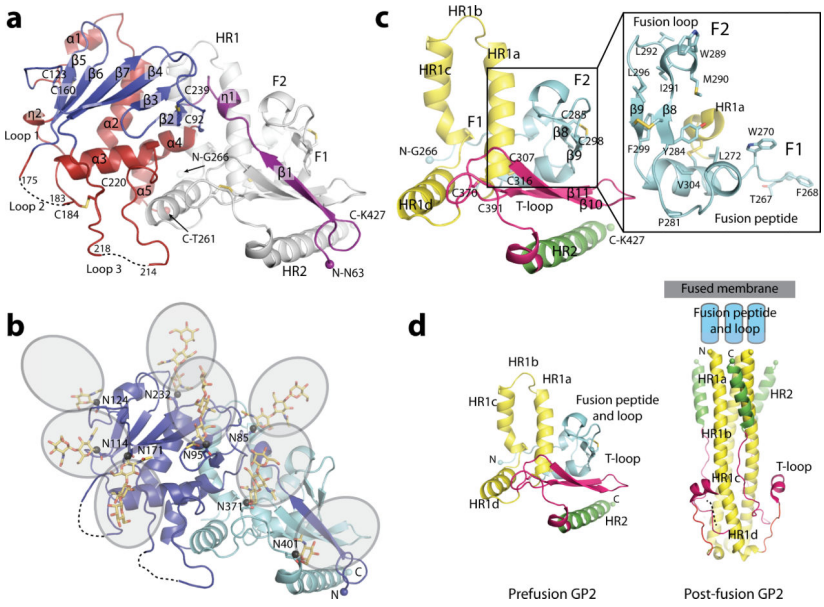

Figure 1. LCMV GP1 and GP2

(a) Ribbon diagram of the GP1 subunit. LCMV GP1 can be divided into three segments: (1) the N-terminal β-strand 1 (purple, at right, interacting with GP2); (2) the upper, β-sheet surface (blue); and (3) the lower helix-loop surface (dark red). The interacting GP2 is shown in grey. **(b)** N-linked glycans visible in the GP1-2 complex crystal structure are illustrated as yellow ball-and-stick, with the linked Asn marked with a dark grey sphere. Transparent ovals are modeled to show the approximate size and orientation of a complex glycan. **(c)** Ribbon diagram of the GP2 subunit. GP2 is in the same orientation as in panel A. LCMV GP2 can be divided into four segments: (I) the fusion region (cyan), which is composed of the fusion peptide (F1), the fusion loop (F2) and the fusion helix; (II) heptad repeat (HR) 1a-d (yellow); (III) the T-loop (magenta); and (IV) HR2 (green). The inset displays F1, F2 and the fusion helix in detail in a different orientation. Residues noted have been shown to be essential for fusion of LASV GPC. **(d)** Comparison between pre- and post-fusion LCMV GP2. In the pre-fusion conformation of LCMV GP2, HR1 (yellow) is broken up into four segments (HR1a-d) and connected to HR2 through the T-loop (pink), which forms the β sheet with β1 of GP1 (panel a). In contrast, in the post-fusion conformation of GP2, HR1 forms a single α helix and the T-loop forms an α helix.

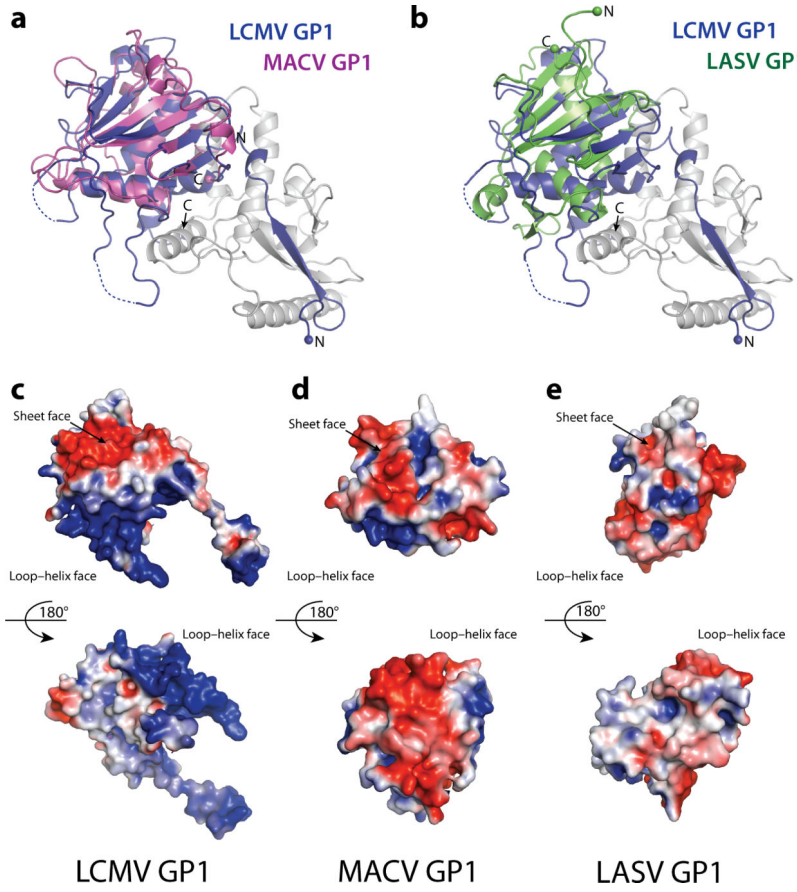

Figure 2. Structural comparison of LCMV GP1 with other arenavirus GP1 subunits

(a) Structural alignment of LCMV GP (blue) and Machupo (MACV) GP1 (magenta, PDB: 3KAS [35]). Despite low sequence similarity of 20%, the GP1 subunits of LCMV and MACV align with an RMSD of 2.08Å. Major differences map to the loops that connect the β-sheet. **(b)** Structural alignment of LCMV GP and Lassa virus (LASV) GP1 (green, PDB: 4ZJF [38]). The GP1 subunits of LCMV and LASV align with an RMSD of 2.85Å. Although the secondary structural elements are generally conserved, the orientations of the GP1 helices, loops and termini are different. **(c)** Electrostatic surface representation of the GP1 subunit of LCMV. **(d)** Electrostatic surface representation of MACV GP1. **(e)** Electrostatic surface representation of LASV GP1. For panels c, d and e the electrostatic potentials were calculated using APBS[56] and range from –2 (red) to +2 (blue) kbT/ec.

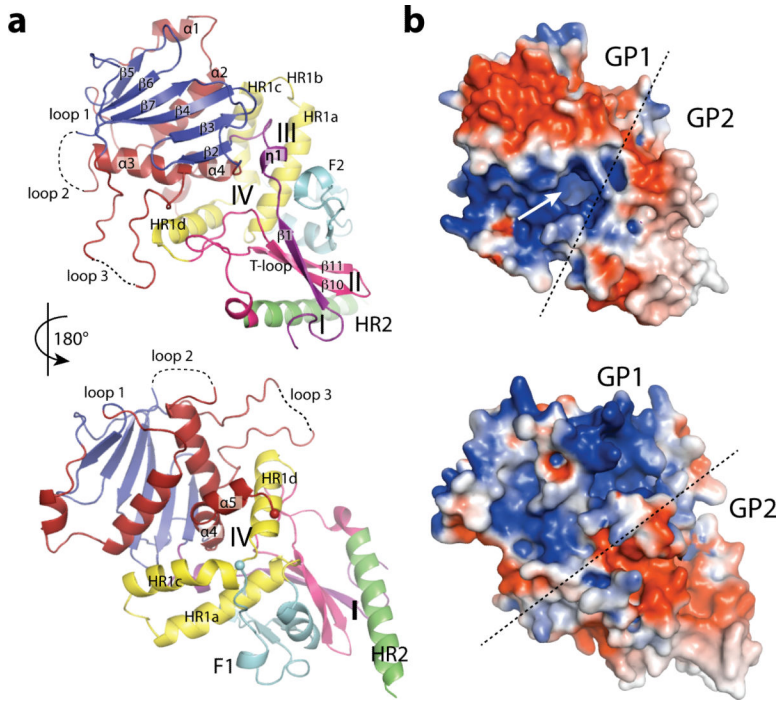

Figure 3. The GP1-GP2 protomer

(a) Cartoon representation colored according to the scheme in Figure 1a and b. The GP1-GP2 interface buries a combined ~5300Å^2. Four interaction sites, encompassing 55 GP1 residues and 73 GP2 residues, are noted: (I) the extreme N-terminal loop of GP1 (purple) makes hydrophobic and hydrophilic contacts to heptad repeat (HR) 2 of GP2 (green); (II) GP1 strand β1 (purple) and GP2 strands β10 and β11 (pink) form an anti-parallel β-sheet; (III) GP1 η1 (purple) and F2 of GP2 (cyan) make both hydrophobic and hydrophilic contacts with one another; and (IV) GP1 α4 (red) occupies a cleft between HR1c and HR1d (yellow) and through primarily hydrophobic contacts, likely anchors these helices in their pre-fusion conformation. **(b)** Electrostatic surface representation of the GP1-GP2 protomer. An approximately 20Å deep basic crevice, indicated with an arrow, is located at the GP1-GP2 interface (denoted with a dotted line). Positive and negative potentials are colored blue and red, respectively. The electrostatic potential was calculated using APBS[56] and ranges from –2 to +2 kbT/ec.

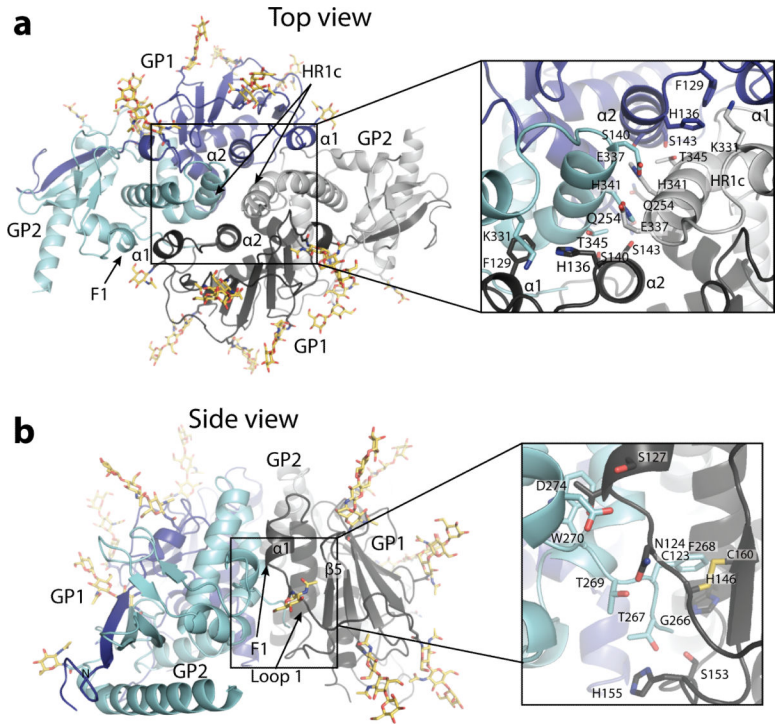

Figure 4. The soluble ectodomain of LCMV forms a dimer in solution and in the asymmetric unit of all crystals

(a) The anti-parallel dimer of GP from the top. Monomer A is colored in dark blue (GP1) and light blue (GP2), while monomer B is colored in dark gray (GP1) and light gray (GP2). N-linked glycans visible in the crystal structure are illustrated in yellow ball and stick. Inset: α2 in the GP1 of each monomer and HR1c in the GP2 of each monomer form a four-helix bundle at the center of the dimeric interaction. **(b)** The GP dimer from the side. Inset: The fusion peptide (F1) of GP2 (cyan) makes both hydrophilic and hydrophobic contacts to the loop that connects β4 to α1 in GP1 (residues 122-127, dark grey) and loop1 (residues 146-155; dark grey). F1 of both monomers A and B form similar interactions to the opposite protomer across the dimer interface.

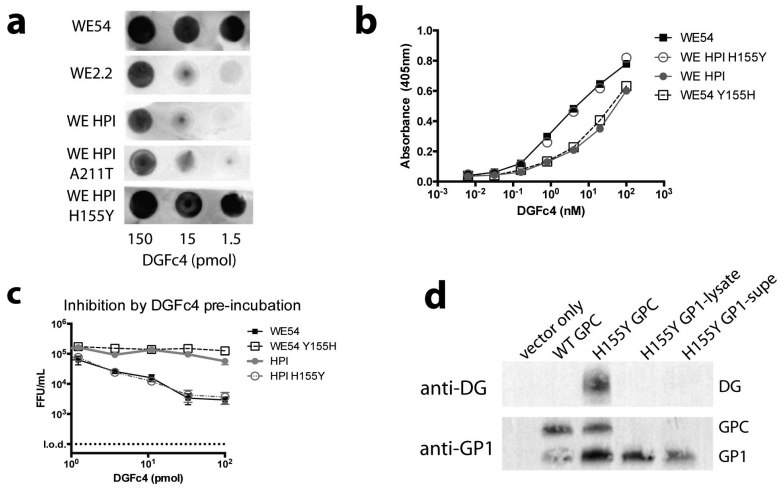

Figure 5. Determinants of receptor binding

(a) Virus-Overlay Protein Binding Assay (VOPBA) showing binding efficiency for different WE strains of LCMV. WE54 is known to exhibit high-affinity binding, while WE2.2 is known to exhibit low-affinity binding [51,52]. **(b)** ELISA showing relative binding affinity for soluble DG. **(c)** Inhibition of viral infectivity in the presence of soluble αDG. Virus infection is shown as fluorescence focus units/mL (FFU/mL). **(d)** Subunit requirements for immunoprecipitation of αDG from cell lysates. Top panel, western blot for DG; bottom panel, western blot for LCMV GP1. For panels b and c error bars indicate s.d. (n=3 technical replicates or cell cultures, respectively). For panel d uncropped blots can be found in Supplementary Data Set 1.

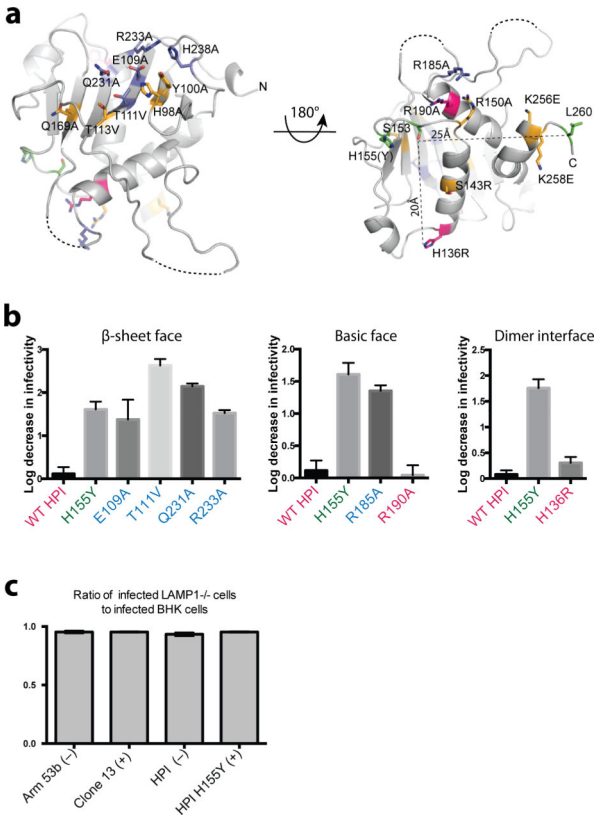

Figure 6. The basic, lower loop face and dimeric interface are required for αDG binding

(a) Cartoon representation of the GP1 subunit of LCMV with residues analyzed shown as sticks. For clarity, the N-terminal strand of GP1 was removed from the representation. Mutations to residues in yellow did not produce virus with titers high enough to analyze further. Viruses bearing mutations to residues in blue (E109A, T111V, R185A, Q231A, and R233A) efficiently bound to αDG. Viruses bearing mutations to residues in magenta (H136R and R190A), failed to bind αDG. Residues previously known to confer high-affinity binding (S135 and L260) as well as Y155 (histidine in the crystallized strain) identified here are colored green. H136 at the dimeric interface is approximately 20Å from the 153, 155 and 190 cluster while L260 at the GP1-GP2 cleavage site is approximately 25Å from these three residues. **(b)** Inhibition of viral infectivity in the presence of soluble αDG. The y axis of each graph is the log decrease in virus infection upon preincubation with soluble αDG, as compared to pre-incubation with PBS. All point mutations were made in the H155Y background, and the H155Y single mutation is shown in each graph for comparison. **(c)** LCMV strains with both high- and low-αDG affinities infect BHK and LAMP1 knock-out cells with equal efficiency. Data shown represents the ratio of LCMV-positive LAMP1 knock-out cells to LCMV-positive BHK cells. Strains of LCMV that bind to αDG with high affinity are indicated by (+) and those that bind to αDG with low affinity are indicated by (–). For panels b and c error bars indicate the s.d. (n=3 cell cultures).

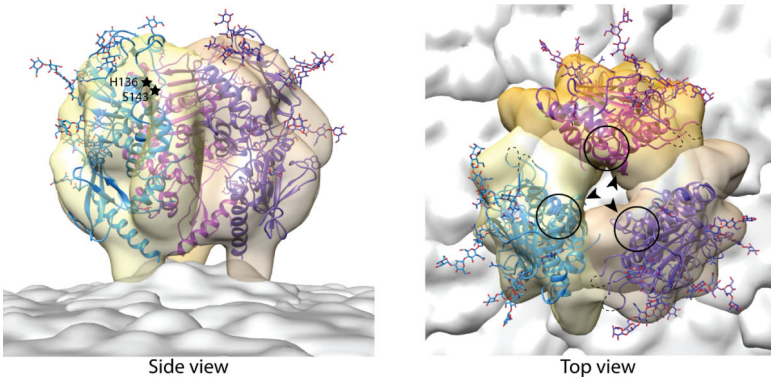

Figure 7. LCMV GP fit into tomographic reconstructions of LASV GPC on the viral surface

Single protomers of prefusion LCMV GPe dimer were docked into the tomographic reconstruction of Lassa virus (LASV) GPC spikes on the virion surface (EMD 3290 [53]). In this docking, all visualized glycans point outward and HR2 and membrane proximal regions orient to the membrane. The panel on the right shows the docked LCMV GP from the side; the panel on the left shows the GP from the top. Regions mapped to αDG binding are noted with a circle on each GP monomer for the cluster of residues 153, 155 and 190 (ranging from approximately 10-20Å from the top of the trimer); with arrows for residue 260 on each GP monomer, which is adjacent to the GP1-GP2 S1P cleavage site (approximately 45Å from the top of the trimer); and with stars for the dimeric interface residues 136 and 143.

Table 1

Data collection, phasing and refinement statistics

	GPe (room temp)[a]	TaBr, GPe (room temp)	GPeFibTryp (frozen) (PDB 5INE)	GPFibTryp (SSAD, frozen)
Data collection				
Space group	I432	I432	I432	I432
Cell dimensions				
a, *b*, *c* (Å)	263.74, 263.74, 263.74	265.46 265.46 265.46	262.33, 262.33, 262.33	263.93, 263.93, 263.93
α, *β*, *γ* (°)	90, 90, 90	90, 90, 90	90, 90, 90	90, 90, 90
Resolution (Å)	45.23-3.75 (3.80-3.75)[b]	44.24-4.65 (4.82-4.65)	47.89-3.5 (3.59-3.5)	48.19-3.83 (3.93-3.83)
R_{pim}	0.045 (0.252)	0.031 (0.468)	0.030 (0.761)	0.027 (0.550)
$I/\sigma I$	8.6 (3.2)	7.7 (1.6)	18.31 (0.9)	18.2 (1.1)
$CC_{1/2}$			99.9 (0.40)	99.9 (0.60)
Completeness (%)	98.0 (99.1)	99.1 (98.0)	99.0 (100.0)	99.9 (99.9)
Redundancy	2 (1.9)	1.1 (1.1)	57.69 (44.6)	62.3 (61.9)
Refinement				
Resolution (Å)			3.5	
No. reflections			19708	
R_{work}/ R_{free}			0.2106/0.2308	
No. atoms			6102	
Protein			5520	
Glycans			582	
Water			0	
B-factors				
Protein			179.90	
Glycans			235.10	
Water				
r.m.s deviations				
Bond lengths (Å)			0.007	
Bond angles (°)			0.940	

[a] Data from three crystals merged for complete data set

[b] Values in parentheses are for highest-resolution shell.